

RESEARCH

Open Access



Higher levels of myelin are associated with higher resistance against tau pathology in Alzheimer's disease

Anna Rubinski¹, Nicolai Franzmeier¹, Anna Dewenter¹, Ying Luan¹, Ruben Smith^{2,3}, Olof Strandberg³, Rik Ossenkoppele^{3,4}, Martin Dichgans^{1,5,6}, Oskar Hansson^{3,7}, Michael Ewers^{1,6*} and the Alzheimer's Disease Neuroimaging Initiative (ADNI)

Abstract

Background: In Alzheimer's disease (AD), fibrillar tau initially occurs locally and progresses preferentially between closely connected regions. However, the underlying sources of regional vulnerability to tau pathology remain unclear. Previous brain-autopsy findings suggest that the myelin levels—which differ substantially between white matter tracts in the brain—are a key modulating factor of region-specific susceptibility to tau deposition. Here, we investigated whether myelination differences between fiber tracts of the human connectome are predictive of the interregional spreading of tau pathology in AD.

Methods: We included two independently recruited samples consisting of amyloid-PET-positive asymptomatic and symptomatic elderly individuals, in whom tau-PET was obtained at baseline (ADNI: $n = 275$; BioFINDER-1: $n = 102$) and longitudinally in a subset (ADNI: $n = 123$, mean FU = 1.53 [0.69–3.95] years; BioFINDER-1: $n = 39$, mean FU = 1.87 [1.21–2.78] years). We constructed MRI templates of the myelin water fraction (MWF) in 200 gray matter ROIs and connecting fiber tracts obtained from adult cognitively normal participants. Using the same 200 ROI brain-parcellation atlas, we obtained tau-PET ROI values from each individual in ADNI and BioFINDER-1. In a spatial regression analysis, we first tested the association between cortical myelin and group-average tau-PET signal in the amyloid-positive and control groups. Secondly, employing a previously established approach of modeling tau-PET spreading based on functional connectivity between ROIs, we estimated in a linear regression analysis, whether the level of fiber-tract myelin modulates the association between functional connectivity and longitudinal tau-PET spreading (i.e., covariance) between ROIs.

Results: We found that higher myelinated cortical regions show lower tau-PET uptake (ADNI: $\rho = -0.267$, $p < 0.001$; BioFINDER-1: $\rho = -0.175$, $p = 0.013$). Fiber-tract myelin levels modulated the association between functional connectivity and tau-PET spreading, such that at higher levels of fiber-tract myelin, the association between stronger connectivity and higher covariance of tau-PET between the connected ROIs was attenuated (interaction fiber-tract myelin \times functional connectivity: ADNI: $\beta = -0.185$, $p < 0.001$; BioFINDER-1: $\beta = -0.166$, $p < 0.001$).

*Correspondence: Michael.Ewers@med.uni-muenchen.de

¹ Institute for Stroke and Dementia Research, University Hospital, LMU Munich, Munich, Germany
Full list of author information is available at the end of the article



© The Author(s) 2022. **Open Access** This article is licensed under a Creative Commons Attribution 4.0 International License, which permits use, sharing, adaptation, distribution and reproduction in any medium or format, as long as you give appropriate credit to the original author(s) and the source, provide a link to the Creative Commons licence, and indicate if changes were made. The images or other third party material in this article are included in the article's Creative Commons licence, unless indicated otherwise in a credit line to the material. If material is not included in the article's Creative Commons licence and your intended use is not permitted by statutory regulation or exceeds the permitted use, you will need to obtain permission directly from the copyright holder. To view a copy of this licence, visit <http://creativecommons.org/licenses/by/4.0/>. The Creative Commons Public Domain Dedication waiver (<http://creativecommons.org/publicdomain/zero/1.0/>) applies to the data made available in this article, unless otherwise stated in a credit line to the data.

Conclusion: Higher levels of myelin are associated with lower susceptibility of the connected regions to accumulate fibrillar tau. These results enhance our understanding of brain substrates that explain regional variation in tau accumulation and encourage future studies to investigate potential underlying mechanisms.

Keywords: Myelin, Myelin water fraction, Tau-PET, Amyloid-PET, Alzheimer's disease, Tau spreading, Resistance

Background

Alzheimer's disease (AD) is defined by the presence of beta-amyloid (A β) plaques and tau neurofibrillary tangles in the brain. The increase in tau pathology is closely associated with neurodegeneration and symptomatic worsening in AD [1–3], demonstrating a key role of tau in the development of dementia. Accumulation of tau pathology during the course of AD occurs gradually in a highly regional and connectivity-dependent manner, as fibrillar tau pathology typically starts in circumscribed brain areas and subsequently progresses to anatomically connected brain areas [4]. The entorhinal cortex is the prevailing epicenter of early fibrillar tau deposition [5–7], from where pathologic tau subsequently progresses to connected higher cortical areas including the medial frontal and posterior parietal cortex [8–12]. Even at advanced disease stages of globally distributed pathologic tau, some brain regions including the somatosensory and the primary motor cortex remain mostly spared [5]. Together, these findings suggest a highly region-dependent susceptibility to tau-pathology that spreads within a network of closely connected brain regions. However, the biological substrates that underlie the region-specific vulnerability to develop tau pathology remain elusive [13]. Their identification could provide key insights into endogenous factors of resistance against the development of fibrillar tau and may be useful for patient-tailored prediction of disease progression.

Here we investigated whether differences in the level of gray-matter and fiber-tract myelin are associated with lower regional fibrillar tau development. The overall rationale is that ontogenetically lower myelinated brain regions and fiber tracts are more vulnerable, where myelin damage may facilitate the development of tau pathology in AD. Myelin constitutes the lipid-rich insulating membrane that ensheaths the nerve fibers [14]. Heterochronicity of nerve-fiber myelination, which can last until the 4th decade of life [15, 16], entails differences in the level of myelination of major fiber tracts and the connecting gray matter regions: primary sensory and motor cortices are more thickly myelinated, whereas late-maturing higher cortical levels of the temporoparietal multimodal association cortices are thinly myelinated [16–18]. In AD, lower myelinated fiber tracts are most vulnerable [19–21]. The impairment of myelin may

enhance the development of pathologic tau [22], potentially through rendering microglia that are overburdened by lipid uptake in a dysfunctional state [23], and thus, a suboptimal immune response to developing AD pathology [24, 25]. A regional correspondence between regions of higher myelin and lower tau pathology has been noted previously based on visual inspection of brain autopsy studies [26]. However, whether regions of higher myelination are associated with lower levels of regional tau pathology and the progressive spreading between connected brain areas has not been tested so far.

Therefore, our first major aim was to assess whether higher myelinated cortical regions show lower susceptibility to the development of fibrillar tau pathology. To this end, we combined an MRI-derived template of myelin in the brain [27] with cross-sectional PET imaging of fibrillar tau, obtained from deeply phenotyped elderly participants from two independent cohorts: the Alzheimer's Disease Neuroimaging Initiative (ADNI) [28] and BioFINDER-1 (<https://clinicaltrials.gov/ct2/show/NCT01208675>).

Our second major aim was to test whether fiber-tract levels of myelin modulated the longitudinal spreading of fibrillar tau in the brain. We previously reported that increases in tau-PET levels are more similar in connected regions showing close functional connectivity [9, 29], supporting the notion that tau spreads preferentially between closely connected brain regions. Here we tested the hypothesis that the level of myelination of the fiber tracts modulates the connectivity-based spreading of tau. Specifically, we hypothesized that higher myelination of fiber tracts is associated with disproportionately lower tau-PET increases in the connected brain regions. In order to address this hypothesis, we combined the myelin maps with MRI-assessed structural and functional connectomes from the human connectome project (HCP) to predict longitudinal tau-PET accumulation over a time period of 1–4 years across both cohorts. Since higher levels of amyloid-PET are a major risk factor of increased cortical tau-PET, we assessed in a sensitivity analysis, whether any associations between myelin and tau-PET can be attributed to amyloid-PET levels. Our study thus investigates in a comprehensive manner in two independent samples myelin as a potentially protective factor against the progression of tau pathology.

Methods

Participants

The current study included participants from two large cohort studies: ADNI and the Swedish BioFINDER-1 study. For our main analyses, participants were selected based on the availability of baseline T1-weighted MRI and [¹⁸F]-AV1451 (florbetapir) tau-PET. For sensitivity analyses, we also acquired all available [¹⁸F]-AV45 (Florbetapir) amyloid-PET in ADNI or [¹⁸F]Flutemetamol amyloid-PET in BioFINDER-1.

For ADNI, the A β status (A β -/+) was determined based on global amyloid-PET levels, where designation of abnormally elevated amyloid deposition (A β +) was defined by the cut-off > 1.11 of global standardized uptake value ratio (SUVR) for [¹⁸F]AV45-Florbetapir-PET, or a global SUVR > 1.08 for [¹⁸F]Florbetaben-PET as established previously [30]. Participants were clinically diagnosed as cognitively normal (CN, Mini-Mental State Exam (MMSE) > 24, Clinical Dementia Rating (CDR) = 0, non-depressed), mildly cognitively impaired (MCI, MMSE > 24, CDR = 0.5, objective memory loss on the education adjusted Wechsler Memory Scale II, preserved activities of daily living), or demented (AD, MMSE of 20 to 26, CDR > 0.5, NINCDS/ADRDA criteria for probable AD). We included a group of participants within the AD spectrum consisting of 119 CN A β +, 97 MCI A β +, and 59 A β + AD dementia participants. As a control sample we included 199 CN A β -/Tau- individuals. Tau negativity was established based on a temporal meta region-of-interest (ROI, including the amygdala, entorhinal cortex, fusiform, parahippocampal, and inferior temporal and middle temporal gyri) cut-off < 1.29, which was shown to discriminate non-AD from AD participants [31]. Ethical approval was obtained by the ADNI investigators at each participating ADNI site, all participants provided written informed consent.

For BioFINDER-1, A β status was determined based on global [¹⁸F]Flutemetamol-PET levels, where abnormally elevated amyloid deposition was defined as a global SUVR cut-off > 0.575 as described previously [32]. The inclusion and exclusion criteria and diagnostic criteria for BioFINDER-1 have been published previously [33]. We included a control sample of 36 CN A β -/Tau-, and a group of participants within the AD spectrum consisting of 30 CN A β +, 26 MCI A β +, and 46 A β + AD dementia participants. All BioFINDER-1 participants gave written informed consent to participate in the study prior to inclusion in the study. Ethical approval was given by the ethics committee of Lund University, Sweden. Imaging procedures were approved by the Swedish Medical Product Agency and the

Radiation Safety Committee at Skåne University Hospital, Sweden.

MRI and PET acquisition and preprocessing in ADNI

In ADNI, structural MRI data was acquired on 3T scanning platforms using T1-weighted MPRAGE sequences using unified scanning protocols across sites (image acquisition procedures can be found on: <http://adni.loni.usc.edu/methods/mri-tool/mri-analysis/>). T1-weighted images and PET scans were taken up to 6 months apart (median interval time = 33 [− 149–176] days).

Tau-PET was assessed with a standardized protocol using 6 × 5 min frames, 75–105 min post-injection of [¹⁸F]-AV1451. Similarly, amyloid-PET was acquired in 4 × 5 min frames, 50–70 min post-injection of [¹⁸F]-AV45. The dynamically acquired frames were coregistered and averaged, and further standardized with respect to the orientation, voxel size, and intensity by the ADNI PET core to produce uniform single tau-PET [34].

T1-weighted MRI images and PET data were preprocessed using the Advanced Normalization Tools (ANTs) toolbox (<http://stnava.github.io/ANTs/>). First, PET images were rigidly co-registered to the participant's T1-weighted MRI image in native space. Using the ANTs cortical thickness pipeline, T1-weighted images were bias field corrected, brain extracted, and segmented into gray matter, white matter, and cerebrospinal fluid tissue maps. Using ANTs high-dimensional warping algorithm [35] the preprocessed T1-weighted MRI images were further non-linearly normalized to Montreal Neurological Institute (MNI) space. By combining the normalization parameters, we further transformed the Schaefer 200 ROI cortical brain atlas parcellation [36] and the reference regions for intensity normalization of PET images from MNI space to native space. Subsequently, the Schaefer parcellation and the reference regions were masked with subject-specific gray matter masks that were binarized at a probability threshold of 0.3.

PET SUVR images were computed by intensity normalizing PET images to the mean tracer uptake of the inferior cerebellar gray matter for tau-PET data, or to the mean tracer uptake of the whole cerebellum for amyloid-PET data, following previous recommendations [37, 38]. Mean PET SUVR values were extracted for each subject for the 200 cortical ROIs (Fig. 1C).

MRI and PET acquisition and preprocessing in BioFINDER-1

In BioFINDER-1, T1-weighted MPRAGE (1 mm isotropic, TR/TE = 1900/2.64 ms) and FLAIR images (0.7 × 0.7 × 5 mm³, 23 slices, TR/TE = 9000/81 ms) were

acquired for all participants on a 3T Siemens Skyra scanner (Siemens Healthineers, Erlangen, Germany).

Tau-PET was acquired 80–100 min after bolus injection of [¹⁸F]AV1451 on a GE Discovery 690 PET scanner (General Electric Medical Systems, Milwaukee, WI, USA).

The image data was processed by the BioFINDER-1 imaging core using a previously described pipeline developed at Lund University [39]. In brief, MRI images were skull stripped using the combined MPRAGE and FLAIR data, segmented into gray and white matter, and non-linearly normalized to MNI space. PET images were attenuation corrected, motion corrected, summed, and coregistered to the MRI images.

In line with the ADNI data, SUVR images were computed by using the inferior cerebellar gray matter as a reference region, and mean tau-PET SUVR values were extracted for each subject for the 200 cortical ROIs.

Transforming tau-PET SUVRs to tau-PET scores

The AV1451 tau-PET tracer shows off-target binding which can confound the measurement of fibrillar tau. In order to enhance the specificity of the tau-PET tracer to assess fibrillar tau, we employed gaussian mixture modeling to tau-PET data to separate the target signal from the background signal as previously described [7, 12]. The underlying rationale is that the variability of regional tau-PET values arises from two sources including off-label bindings observed mostly in regions free of fibrillar tau and those with abnormally increased fibrillar tau (such as present in A β + participants), resulting in a bimodal distribution of ROI values centered around a mean of off-label tracer binding and a distribution of ROI values centered around a mean of on-target tracer binding. For a given participant's ROI value, a tau-positivity probability score (i.e. the probability that the tau-PET ROI value reflects abnormal fibrillar tau) can be calculated based on the percentiles of the off-label and target ROI value distributions. In the current study, we applied gaussian mixture modeling to 200-ROI tau-PET SUVRs across participants separately in each study including ADNI and BioFINDER-1. We computed for each participant and ROI the probability to belong either to the off-target or on-target distribution as described previously

by us [12]. The resulting tau-positivity probabilities were then multiplied by the original tau-PET SUVRs in order to obtain tau-positivity weighted tau-PET scores.

Assessment of covariance in tau change

Using longitudinal tau-PET data, we then computed the annual tau change within each of the 200 ROIs for each participant. This was done by computing for each ROI the baseline vs follow-up differences in tau-PET scores divided by the time (in years) between the tau scans. Covariance in tau change (the correlation between tau change levels between pair of regions) was computed by correlating regional tau-PET score change levels between each pair of ROIs across participants using Spearman's correlation. Resulting in a single 200 \times 200 sized covariance in tau change matrix for both cohorts. We set autocorrelations to zero and further Fisher-z-transformed all correlations. Similarly, for sensitivity analyses, we computed the covariance in amyloid-PET change as well as a covariance in tau change, using Spearman's partial correlation controlled for age, sex, education, APOE ϵ 4 status, diagnosis, and site.

Assessment of cortical and fiber tract myelin water fraction (MWF)

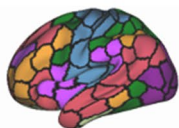
Cortical and fiber tracts myelination was determined based on a normative MWF atlas derived from myelin water imaging of healthy individuals ($n=50$, mean age 25 years) [27]. To determine the regional cortical distribution, we applied a neocortical 200 ROI brain parcellation (Fig. 1A; 36) to the myelin water atlas and extracted the regional mean MWF within each of the 200 ROIs (Fig. 1B). To determine the myelin content within the fiber-tracts connecting each pair of ROIs, first, we obtained minimally preprocessed diffusion-weighted images (DWI) [40] from 100 participants of the human connectome project (HCP). We further used a multi-shell multi-tissue constrained spherical deconvolution and probabilistic tractography pipeline, as previously described [12]. Using the same 200 ROI parcellation, we defined nodes and assigned for each pair of ROIs the reconstructed fiber tract streamlines (Fig. 1H). The myelin water atlas was then applied to the reconstructed streamlines, and the mean myelin value along the streamlines between each of the two regions

(See figure on next page.)

Fig. 1 Analysis flow chart. **A** Surface rendering of the 200-ROI brain atlas, based on which we estimated **B** cortical MWF and **C** group-level tau-PET scores, which were further vectorized (**D**) and spatially correlated. **E** The same brain atlas shown in (**A**) was applied to each participant's tau-PET score change rates, individual values were vectorized and all possible pairs of ROIs across participants were correlated to obtain a covariance in tau-PET score change matrix (**F**). **G** Using the 200 ROI brain atlas shown in (**A**), resting-state fMRI functional connectivity was assessed on 100 participants of the human connectome project (HCP). **H** Diffusion MRI from the HCP was used to estimate the fiber-tracts between each pair of ROIs in the brain atlas shown in (**A**). **I** The MWF atlas was overlaid to extract regional MWF values of underlying fiber tracts. **J** Linear regression analysis was performed with the covariance in tau-PET score change as the dependent variable, and the interaction of functional connectivity by MWF in fiber-tract as the predictor. In a sensitivity analysis, we further controlled the above-mentioned analyses for regional amyloid-PET levels or the covariance in amyloid-PET change (not shown)

Association between cortical myelin water fraction (MWF) and tau-PET

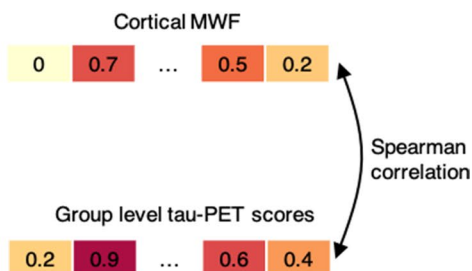
A. 200-ROI brain atlas



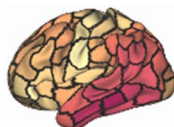
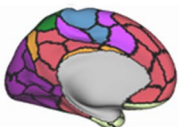
B. Parcellated MWF atlas



D. Vectorized ROI values



C. Cross-sectional Tau-PET



Interaction functional connectivity x MWF on rate of change in tau accumulation

E. Tau-PET score change rate



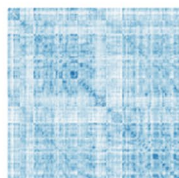
Vectorize tau-PET score change rate for each participant

Subject 1	0.3	1.0	...	0.1	0.4
Subject 2	0.9	0.2	...	0.4	0.8
...
Subject N	0.1	0.7	...	0.3	0.6

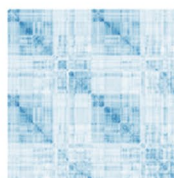
Correlate all possible pairs of ROIs across participants to obtain 200x200 tau change covariance matrix

Spearman correlation

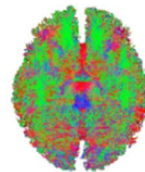
F. Covariance in Tau-PET score change matrix



G. Functional connectivity (HCP)



H. Diffusion MRI based fiber tracking (HCP)

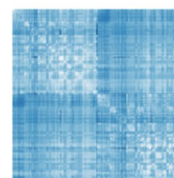


Extract fiber tracts between ROIs



Overlay MWF atlas to extract regional MWF values in fiber tracts connecting all possible pairs of ROIs

I. MWF in fiber-tracts



J: Model: Covariance in Tau PET change ~ Functional Connectivity x MWF in fiber tracts

Fig. 1 (See legend on previous page.)

was extracted. This resulted in a 200×200 matrix of the mean MWF in fiber tracts between each pair of ROIs. From the resulting 100 MWF matrices, we computed the group-average MWF in fiber tracts matrix (see Fig. 1I).

Assessment of functional connectivity

To determine a functional connectivity template, we downloaded spatially normalized, minimally preprocessed resting-state fMRI images from the same 100 participants of the HCP. We then applied detrending, band-pass filtering (0.01–0.08 Hz), despiking, and motion correction to the HCP resting-state data. For each individual, we assessed the functional connectivity values by Fisher- z -transformed Pearson-moment correlations between all possible ROI pairs in the Schaefer parcellation. From the resulting 100 functional connectivity matrices, we computed the group-average functional connectivity matrix (Fig. 1G).

Statistics

Within each cohort, subject characteristics were compared between groups using Kruskal–Wallis for continuous measures (post hoc Dunn's tests adjusted for multiple comparisons) or Chi-squared (χ^2) tests for categorical measures.

In order to test the association between cortical MWF and group-averaged tau-PET scores in corresponding gray matter ROIs, we computed a spatial correlation using Spearman's rank correlation (Fig. 1B–D) separately for ADNI and BioFINDER-1. As sensitivity analyses, we first repeated this analysis using tau-PET SUVRs as the dependent variable, and secondly we tested whether the association differed by APOE $\epsilon 4$ status ($\epsilon 4$ allele carriers vs non-carriers). To this end, we first stratified participants by APOE $\epsilon 4$ status and determined the bootstrapped distribution of the correlation coefficients (ρ) between MWF and tau-PET scores for each of the two APOE groups. Next, we randomly sampled from the participants pool with replacement in each of the APOE groups, and we computed the 95% confidence intervals (CI) of the ρ -value distribution within each of the groups, using 1000 bootstrapping iterations.

Next, we assessed whether the myelin levels of the fiber tracts are a modulating factor of connectivity-based spreading of tau. To that end, using linear regression we tested the interaction functional connectivity by MWF in fiber-tracts on the covariance in tau-PET score change separately for ADNI and BioFINDER-1. In additional analyses, we controlled the assessment of

covariance in tau change for age, sex, APOE $\epsilon 4$ status, diagnosis, and site.

Finally, in order to assess whether the observed associations in the current study are driven by regional amyloid pathology, we repeated the above-mentioned analyses controlling for baseline amyloid-PET levels or covariance in amyloid-PET change based on the analysis.

All statistical analyses were performed using R statistical software. Brain surface renderings were created in a connectome workbench. All effects were considered significant when meeting an α -threshold of 0.05.

Results

We included a total of 612 participants consisting of non-demented and demented individuals with biomarker evidence of AD including elevated amyloid-PET accumulation ($A\beta+$, ADNI: $n=275$; BioFINDER-1: $n=102$) and CN controls without elevated amyloid-PET and tau-PET ($A\beta$ -/Tau-, ADNI: $n=199$; BioFINDER-1: $n=36$, see Table 1).

Higher cortical myelin is associated with lower tau-PET

Our first aim was to test in a cross-sectional analysis whether higher myelin levels in gray matter regions were associated with lower tau-PET uptake in spatially corresponding regions. To this end, we first applied a 200 ROIs cortical brain-parcellation atlas (Fig. 1A) to a spatially normalized MRI-based MWF template from cognitively normal healthy adults ($n=50$, mean age 25 years) [27] in order to extract normative MWF ROI values from cortical brain regions (Fig. 1B). Next, we obtained subject-level tau-PET SUVRs from the same 200 ROI based on the tau-PET scans in the ADNI and BioFINDER-1 cohorts (Fig. 1C). The tau-PET ROI SUVRs were weighted by tau-positivity probability [7, 12] in order to reduce the influence of off-target background binding (henceforth called tau-PET scores, see Supplementary Fig. 1). We used spatial correlation to assess whether those gray matter ROIs with higher MWF levels show lower tau-PET scores in AD (Fig. 1D). As hypothesized, we found that higher ROI-MWF values were associated with lower tau-PET scores in corresponding gray matter ROIs for $A\beta+$ participants in both ADNI ($\rho = -0.267$, $p < 0.001$; Fig. 2A) and BioFINDER-1 ($\rho = -0.175$, $p = 0.013$; Fig. 2B). The analysis in the CN $A\beta$ -/Tau- participants was not significant both in ADNI ($\rho = -0.13$, $p = 0.067$; Fig. 2A) and BioFINDER-1 ($\rho = 0.027$, $p = 0.7$; Fig. 2B), suggesting that the association between MWF and tau-PET scores is robust only in the group with biomarker evidence of AD.

Table 1 Sample demographics, mean (SD)

ADNI					
	CN Ab-/Tau- (n=199)	CN Ab+ (n=119)	MCI Ab+ (n=97)	AD dementia (n=59)	p-value
Age, years	70.88 (6.40) ^{†,‡,§}	74.64 (7.39) [*]	74.77 (7.40) [*]	76.20 (9.33) [*]	<0.001
Sex, M/F	72 / 127	44 / 75	51 / 46	31 / 28	0.011
Education, years	16.78 (2.28) [§]	16.68 (2.38) [§]	16.11 (2.46)	15.44 (2.41) ^{*,†}	<0.001
MMSE	29.19 (1.07) ^{†,§}	28.91 (1.36) ^{†,§}	27.49 (2.19) ^{*,†,§}	22.19 (3.96) ^{*,†,‡}	<0.001
APOE e4 carriers -/+ ^a	136- / 51+ ^{†,‡,§}	54- / 60+ [*]	29- / 53+ [*]	18- / 32+ [*]	<0.001
Mean tau-PET follow-up, years ^b	1.72 (0.53)	1.64 (0.57)	1.45 (0.71)	1.37 (0.49)	0.299
BioFINDER-1					
	CN Ab-/Tau- (n=36)	CN Ab+ (n=30)	MCI Ab+ (n=26)	AD dementia (n=46)	p-value
Age, years	73.86 (7.27)	73.80 (7.44)	71.73 (9.72)	71.43 (7.34)	0.274
Sex, M/F	19 / 17	12 / 18	18 / 8	25 / 21	0.187
Education, years	12.42 (3.80)	11.93 (3.72)	12.21 (3.93)	12.22 (3.75)	0.928
MMSE	28.86 (1.10) ^{†,§}	28.83 (1.15) ^{†,§}	25.58 (3.06) ^{*,†,§}	20.96 (4.87) ^{*,†,‡}	< 0.001
APOE e4 carriers -/+	29- / 7+ ^{†,‡,§}	8- / 22+ [*]	6- / 20+ [*]	19- / 27+ [*]	< 0.001
Mean tau-PET follow-up, years ^c	2.03 (0.47)	1.94 (0.32)	1.82 (0.12)	1.87 (0.34)	0.470

Abbreviations: Aβ Amyloid-beta, AD Alzheimer's disease, APOE Apolipoprotein E, CN Cognitively normal, F Female, M Male, MCI Mild cognitive impairment, MMSE Mini-Mental State Exam

^aavailable for 187 CN Aβ-/Tau-, 114 CN Aβ+, 82 MCI Aβ+, and 50 AD dementia

^bsubsample of 35 CN Aβ-/Tau-, 60 CN Aβ+, 39 MCI Aβ+, and 24 AD dementia

^csubsample of 16 CN Aβ-/Tau-, 14 CN Aβ+, 7 MCI Aβ+, and 18 AD dementia

^{*}Significantly different from CN Aβ-/Tau-

[†]Significantly different from CN Aβ+

[‡]Significantly different from MCI Aβ+

[§]Significantly different from AD dementia (significant after applying a Bonferroni-corrected α-threshold of 0.0125)

In a sensitivity analysis, we analyzed whether the associations differed between groups stratified by APOE ε4 status. In a stratified analysis, the 95% CIs of the bootstrapped rho values of the association between ROI-MWF values and tau-PET scores overlapped between the APOE-ε4 carriers and APOE-ε4 non-carriers both in ADNI (APOE-ε4 carriers: CI [-0.375, -0.218], APOE-ε4 non-carriers: CI [-0.318, -0.05]) and in BioFINDER-1 (APOE-ε4 carriers: CI [-0.187, -0.019], APOE-ε4 non-carriers: CI [-0.286, -0.14]), indicating that there is no significant difference between the groups.

Furthermore, in an additional sensitivity analysis, we used tau-PET SUVRs instead of tau-PET scores. We found that higher ROI-MWF values were associated with lower tau-PET SUVRs in corresponding gray matter ROIs for Aβ+ participants in both ADNI (rho = -0.348, p < 0.001; Supplementary Fig. 2A) and BioFINDER-1 (rho = -0.255, p < 0.001; Supplementary Fig. 2B).

Higher myelination of fiber tracts attenuates rates of longitudinal tau-PET increase in connected regions

We and others previously reported that tau-PET preferentially progresses between closely connected brain

regions [9]. Here, we tested whether myelination of fiber tracts modulates the rate of connectivity-dependent tau-PET accumulation in Aβ+ participants. We addressed this hypothesis in a subset of Aβ+ participants who had longitudinal tau-PET (ADNI: n = 123, mean FU interval = 1.53 [0.69–3.95] years; BioFINDER-1: n = 39, mean FU interval = 1.87 [1.21–2.78] years). Adopting our previously established approach to assess connectivity-based tau accumulation [9, 29], we first estimated the functional connectivity between each of the ROIs (Fig. 1G). Next, in order to determine whether functionally connected regions show similar rates of tau accumulation, we computed the covariance in tau-PET score change (i.e., the level of similarity in tau change between two regions; Fig. 1E, F). We then determined the level of myelin in the fiber tracts connecting each pair of ROIs to test whether myelin levels modulate the association between the functional connectivity and the change in tau-PET in the connected ROIs. To this end, we obtained the normative fiber-tract myelin levels from the same MWF template as used before, this time masked by an ROI-to-ROI structural connectivity matrix based on diffusion MRI data from 100 healthy individuals assessed in the HCP

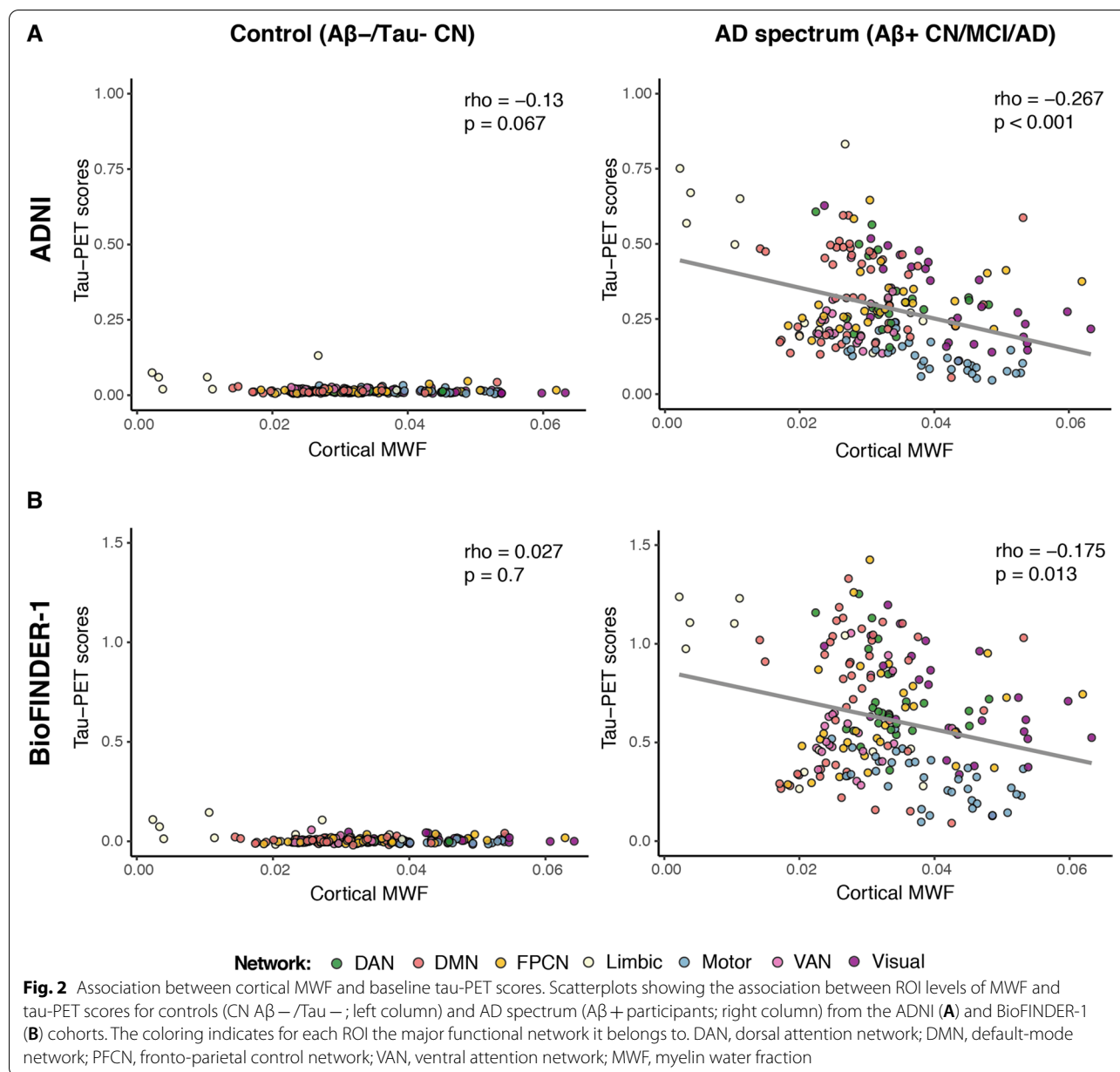
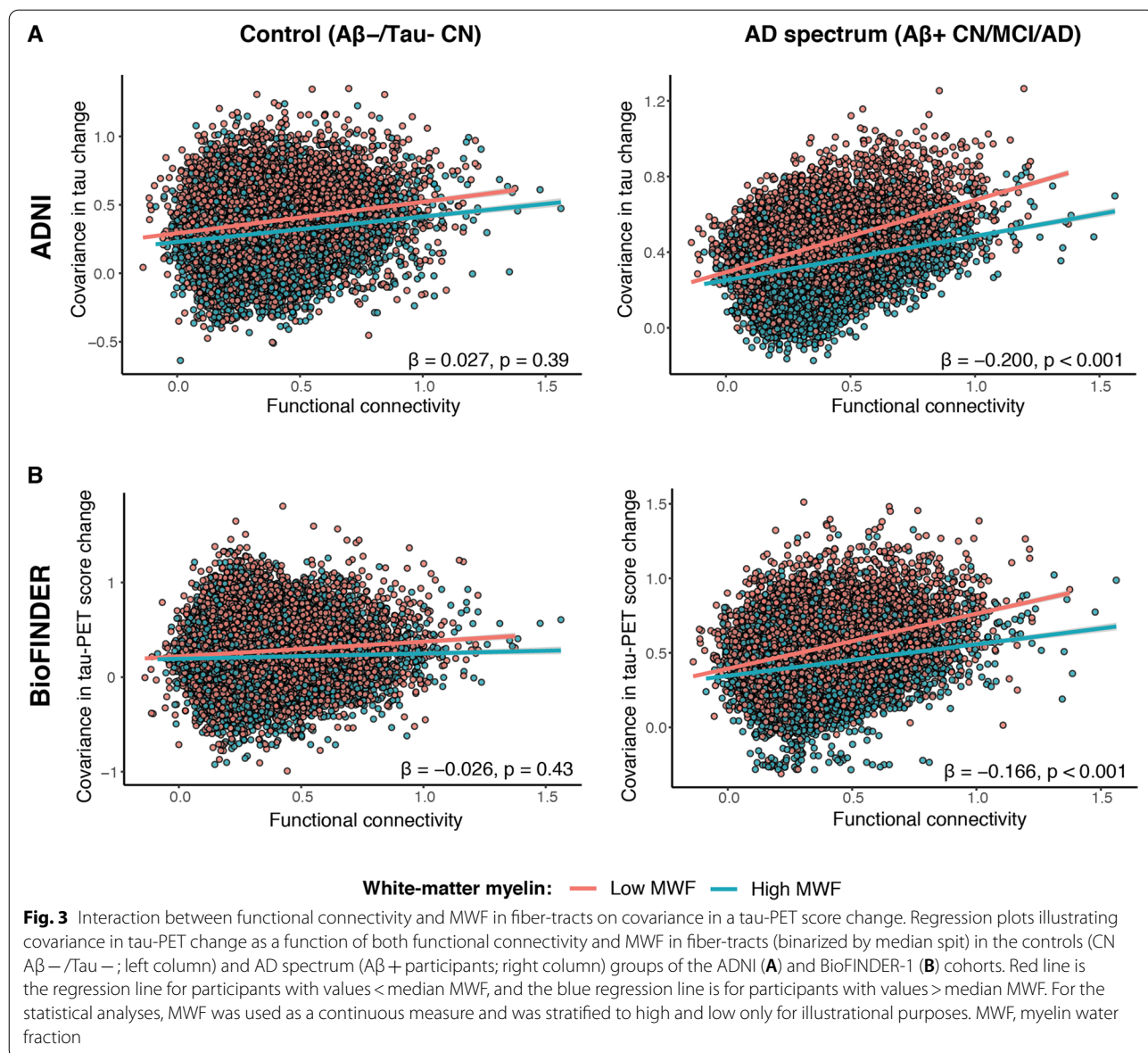


(Fig. 1H, I). In a linear regression analysis, we tested the interaction functional connectivity by MWF in fiber-tracts as predictors of the covariance in tau change matrix (Fig. 1J). We found a significant interaction of functional connectivity by fiber-tract MWF on covariance in tau change in both ADNI ($\beta = -0.185, p < 0.001$; Fig. 3A) and BioFINDER-1 ($\beta = -0.166, p < 0.001$; Fig. 3B), where regions that were connected by higher myelinated fiber tracts showed a lower association between functional connectivity and the rate of change in tau-PET scores. Results remained consistent when controlling the assessment of covariance in tau change for age, sex, education, APOE $\epsilon 4$ status, diagnosis, and site (ADNI: $\beta = -0.114,$

$p < 0.001$; BioFINDER-1: $\beta = -0.066, p = 0.029$). These associations were not significant in the control groups (ADNI: $\beta = 0.027, p = 0.39$; BioFINDER-1: $\beta = -0.026, p = 0.43$; Fig. 3A, B). These results suggest that in the groups with biomarker evidence of AD, myelin is associated with an attenuated rate of connectivity-dependent tau-PET increase over time.

The role of amyloid deposition in the associations between tau and MWF

In sensitivity analyses, we tested whether the above-mentioned associations were driven by regional amyloid pathology. Amyloid-PET was acquired in close temporal



proximity to baseline tau-PET in 168 Aβ⁺ participants in ADNI (mean interval = 20.5 [1–156] days) and in all participants in BioFINDER-1 (cross-sectional amyloid PET only).

First, we tested the association between cortical MWF and tau-PET scores, controlling for regional amyloid-PET SUVRs. We found that higher cortical MWF was associated with lower tau-PET scores in corresponding gray matter ROIs independent of amyloid-PET in ADNI ($\rho = -0.21, p = 0.003$), but the association no longer reached significance in BioFINDER-1, although exploratory analysis showed that the association between cortical MWF and tau-PET was consistently independent of amyloid-PET in the non-demented group (CN Aβ⁺ and MCI Aβ⁺) in both ADNI ($\rho = -0.241, p = 0.0006$) and

BioFINDER-1 ($\rho = -0.141, p = 0.046$). These results suggest at the descriptive level, that especially in the early stage of AD, when tau-PET has not yet globally spread, the spatial association between myelin and tau deposition in the gray matter is independent of Aβ.

Next, we tested whether the association between higher fiber-tract MWF and lower connectivity-dependent longitudinal tau-PET accumulation remained significant in ADNI (no longitudinal amyloid-PET was obtained in BioFINDER-1). When controlling for the covariance in amyloid-PET change, the interaction functional connectivity by MWF in fiber tracts on covariance in tau change remained significant ($\beta = -0.07, p = 0.005$), suggesting that the association between higher levels of myelin and

lower tau-PET accumulation was not dependent on differences in A β .

Discussion

We combined for the first time high-resolution MRI-assessed mapping of myelin, resting-state fMRI functional connectomics, and subject-level tau-PET imaging in two independent samples of deeply characterized elderly individuals with biomarker evidence of AD. In the current study, we found a close spatial association between higher myelin levels and lower cross-sectional and longitudinal increase in tau-PET accumulation. Specifically, our first major finding showed that higher levels of myelin as assessed by MWF were consistently associated with lower tau-PET uptake in corresponding gray matter regions. This result suggests that brain regions with higher myelin levels are less prone to accumulate fibrillar tau. Our second major finding concerned the longitudinal progression of tau-PET between connected brain areas. We revealed that higher MWF levels in fiber tracts were associated with lower connectivity-dependent rates of tau-PET increases. This result suggests that higher fiber-tract myelination is associated with attenuated spreading of fibrillar tau in the brain. Although we caution against a causative interpretation, our current findings suggest that higher regional levels of myelin are associated with higher resistance against the susceptibility and rate of progression of fibrillar tau.

Our findings significantly advance previous qualitative brain autopsy studies that suggested an association between myelin and tau pathology [21, 26, 41], but were limited to qualitative visual inspection of sparsely sampled post-mortem data of tau pathology and myelin maps [26]. Here, using a longitudinal tau-PET approach, we show that higher fiber-tract myelination is associated with a lower connectivity-dependent rate of tau-PET progression. We thus advance previous findings on the association between the connectivity-based prediction of faster tau-PET accumulation in regions which are closely connected [9, 12, 42, 43], demonstrating that such connectivity-related increases in tau-PET accumulation are attenuated for regions connected by higher myelinated fiber-tracts. Together, our findings strongly support the notion that higher myelination is associated with lower susceptibility to tau accumulation and contribute to explain why some regions are highly vulnerable to tau pathology whereas others are relatively spared.

The mechanisms that may underlie a protective effect of higher myelin on lower tau pathology are poorly understood. A possible explanation is that lower myelinated axons are more prone to myelin damage, where subsequent remyelination processes entail higher phosphorylation of tau and subsequent formation of fibrillar

tau [44, 45]. Myelin damage has been observed previously in histochemical and neuroimaging studies in AD [46–49], and recent single-cell studies provide converging results showing that alterations in oligodendrocytes, a cell type involved in myelination, are prominent in AD [50, 51]. Experimentally induced myelin damage leads to the activation of tau-targeting kinases entailing hyperphosphorylation of tau [22, 52], and could trigger further spreading of tau pathology [53, 54]. At the molecular level, the Fyn kinase, which is a key signaling molecule that binds tau in axonal microtubules [55], becomes activated during remyelination efforts triggered by myelin disturbances [56]. In mouse models of tauopathies, blocking Fyn kinase completely prevented the formation of neurofibrillary tangles [57]. Together, these results suggest the possibility that myelin-triggered Fyn kinase may play a role in the formation of tau tangles in AD. Alternatively, myelin alterations may enhance the development of tau pathology via increasing microglia activity. Previous research showed that myelin changes are associated with increased disease-associated microglia (DAM) gene-expression signatures triggering microglial uptake of myelin lipids [24]. The uptake of lipid droplets from myelin debris may render microglia overburdened and senescent [23, 58]. Furthermore, myelin-related microglia activation increases the inflammasome [23], which facilitates the development of fibrillar tau pathology [59]. Therefore, myelin alterations that occur preferentially in lower myelinated brain regions (for review see [60]) can trigger a type of microglia activation that entails a suboptimal response to developing tau pathology and thus indirectly enhances tau pathology.

Myelin damage may also lead to enhanced development of amyloid plaques [21]. Recent studies in transgenic mouse models of amyloid pathology suggest that acute demyelination may occur *upstream* of amyloid deposition by interfering with a TREM2-related microglia activation signature, thus leading to enhanced amyloid deposition [25]. Thus, more vulnerable, thinner myelinated regions may engage in dysfunctional microglial activity resulting in less efficient removal of AD pathology. However, our current results do not suggest that regional differences in the level of amyloid-PET explain the association between brain regions connected by lower myelinated fiber tracts and regional tau-PET accumulation. In the larger ADNI sample, the association between MWF in gray matter or fiber tracts with tau-PET remained significant after controlling for amyloid-PET, although in BioFINDER-1 there was a nominal association of cortical MWF with tau-PET only in nondemented participants. These results suggest that any association between myelin and A β deposition unlikely accounts for the association with tau-PET.

In summary, regions with higher myelination may be less vulnerable to late-life myelin alterations and thus a pathological cascade that includes the development of AD pathologies.

Our findings have important clinical implications. First, our results suggest that myelin adds to the connectivity-based prediction of regional increases in tau-PET [9, 12], and may thus contribute to patient-tailored outcome parameters on treatment effects on tau-PET changes [61]. Second, the current findings suggest myelin to be a potential target for the prevention and treatment of AD [62]. Myelination is a druggable target [63, 64], and thus, pharmacological stimulation of myelination is a putative therapeutic target in AD. Clemastine, a licensed H1 histamine, has been recently shown to enhance the differentiation of oligodendrocyte precursor cells and myelination [65, 66], where clinical trials repurposing clemastine for the treatment of multiple sclerosis have shown improvement of symptoms [67]. Treatment of transgenic mouse model of A β with clemastine showed alleviated oligodendrocyte progenitor cell and myelin loss, reduced A β deposition and ameliorated memory loss [45, 68]. Together, these results suggest that myelin is a putative drug target in AD and encourage future studies to test the effect of myelin treatment on tau pathology.

Limitations

Several caveats should be considered when interpreting our results. First, current MRI acquisition sequences are imperfect measures of myelin and are susceptible to the iron content in the brain tissue [69]. However, we employed an MR-based myelin water imaging [27], which has been extensively validated by histopathology [70, 71] and shows one of the strongest associations with post-mortem assessed myelin levels compared to alternative MRI measures of myelin [72]. Also, we avoided a potential confounding of the MRI myelin signal with disease-related iron and white matter alterations by using a myelin water imaging template that was obtained in healthy individuals [27]. Therefore, the current findings are unlikely to be driven by spurious associations with off-target MRI signals. Second, in the current study, we used a myelin template from healthy individuals ($n=50$, mean age 25 years) and did not assess myelin changes in the AD patients. While the use of a template reflects more accurately pre-morbid inter-regional differences in myelination, demyelination has been observed in aging [73], small vessel disease [74], and AD [75] in association with amyloid plaques [48] and fibrillar tau [46]. Hence, myelin changes may alter the rate of change in tau-PET. Patient-specific levels of myelin were not available in the current study, but the hypothesis is that regions with lower levels of myelin are more prone to undergo

demyelination which then triggers the development of tau pathology.

Conclusions

Our findings show for the first time that higher myelination is associated with slower tau progression in AD. Our results demonstrate that myelin maps inform the connectome-based prediction of pathology-spreading models, and thus also pave the way for future clinical studies in which the individual interregional differences in myelination can be assessed for patient-tailored prediction of disease progression.

Abbreviations

AD: Alzheimer's disease; ADNI: Alzheimer's Disease Neuroimaging Initiative; ANTs: Advanced normalization tools; APOE: Apolipoprotein E; A β : Beta-amyloid; CDR: Clinical Dementia Rating; CN: Cognitively normal; DWI: Diffusion-weighted imaging; FU: Follow-up; HCP: Human connectome project; MCI: Mild cognitive impairment; MNI: Montreal Neurological Institute; MMSE: Mini-Mental State Examination; MRI: Magnetic resonance imaging; MWF: Myelin water fraction; PET: Positron emission tomography; ROI: Region of interest; SUVR: Standard uptake value ratio.

Supplementary Information

The online version contains supplementary material available at <https://doi.org/10.1186/s13195-022-01074-9>.

Additional file 1: Supplementary figure 1. Brain renderings of cortical myelin within the MWF template and tau-PET scores among controls and AD participants. **Supplementary figure 2.** Association between cortical MWF and baseline tau-PET SUVRs.

Acknowledgements

Parts of the data used in the preparation of this manuscript were obtained from the ADNI database (adni.loni.usc.edu). As such, the investigators within the ADNI study contributed to the design and implementation of ADNI and/or provided data but did not participate in the analysis or writing of this paper. A complete list of ADNI investigators can be found at: https://adni.loni.usc.edu/wp-content/uploads/how_to_apply/ADNI_Acknowledgement_List.pdf

Authors' contributions

AR: study concept and design, data processing, statistical analysis, interpretation of the results, and writing the manuscript. N.F.: data processing and critical revision of the manuscript; A.D.: data processing and critical revision of the manuscript. Y.L.: data processing and critical revision of the manuscript. R.S.: critical revision of the manuscript. O.S.: critical revision of the manuscript. R.O.: critical revision of the manuscript. M.D.: critical revision of the manuscript. O.H.: critical revision of the manuscript. M.E.: study concept and design, interpretation of the results, and writing the manuscript. The authors read and approved the final manuscript.

Funding

Open Access funding enabled and organized by Projekt DEAL. The study was supported by the German Center for Neurodegenerative Diseases (DZNE), and the Deutsche Forschungsgemeinschaft (DFG, German Research Foundation) grant for major research instrumentation (INST 409/193-1 FUGG). ADNI data collection and sharing for this project was funded by the ADNI (National Institutes of Health Grant U01 AG024904) and DOD ADNI (Department of Defense award number W81XWH-12-2-0012). ADNI is funded by the National Institute on Aging, the National Institute of Biomedical Imaging, and Bioengineering, and through contributions from the following: AbbVie, Alzheimer's Association; Alzheimer's Drug Discovery Foundation; Araclon Biotech; BioClinica, Inc.; Biogen; Bristol-Myers Squibb Company; CereSpir, Inc.; Cogstate; Eisai Inc.; Elan Pharmaceuticals, Inc.; Eli Lilly and Company; EuroImmun; F. Hoffmann-La

Roche Ltd and its affiliated company Genentech, Inc.; Fujirebio; GE Healthcare; IXICO Ltd.; Janssen Alzheimer Immunotherapy Research & Development, LLC.; Johnson & Johnson Pharmaceutical Research & Development LLC.; Lumosity; Lundbeck; Merck & Co., Inc.; Meso Scale Diagnostics, LLC.; NeuroRx Research; Neurotrack Technologies; Novartis Pharmaceuticals Corporation; Pfizer Inc.; Piramal Imaging; Servier; Takeda Pharmaceutical Company; and Transition Therapeutics. The Canadian Institutes of Health Research is providing funds to support ADNI clinical sites in Canada. Private sector contributions are facilitated by the Foundation for the National Institutes of Health (www.fnih.org).

Availability of data and materials

The data used in this study were obtained from the Alzheimer's disease Neuroimaging Initiative and are available from the ADNI database (adni.loni.usc.edu) upon registration and compliance with the data usage agreement. Data from the BioFINDER-1 cohort are available from the authors upon request. Resting-state and diffusion-weighted data of the HCP cohort are freely available online (<https://db.humanconnectome.org>). MWF template is freely available online (<https://sourceforge.net/projects/myelin-water-atlas/>).

Declarations

Ethics approval and consent to participate

For ADNI, ethical approval was obtained by the ADNI investigators; all study participants provided written informed consent. For BioFINDER-1, ethical approval was given by the ethics committee of Lund University, Sweden. Imaging procedures were approved by the Swedish Medical Product Agency and the Radiation Safety Committee at Skåne University Hospital, Sweden.

Consent for publication

Not applicable.

Competing interests

M.E and N.F. receive research funding from Eli Lilly; M.E. serves as a consultant for Eli Lilly. The other authors declare that they have no competing interests.

Author details

¹Institute for Stroke and Dementia Research, University Hospital, LMU Munich, Munich, Germany. ²Department of Neurology, Skåne University Hospital, Lund, Sweden. ³Clinical Memory Research Unit, Department of Clinical Sciences Malmö, Lund University, Lund, Sweden. ⁴Department of Neurology, Alzheimer Center Amsterdam, Amsterdam Neuroscience, Vrije Universiteit Amsterdam, Amsterdam UMC, Amsterdam, Netherlands. ⁵Munich Cluster for Systems Neurology (SyNergy), Munich, Germany. ⁶German Center for Neurodegenerative Diseases (DZNE), Munich, Germany. ⁷Memory Clinic, Skåne University Hospital, Malmö, Sweden.

Received: 11 May 2022 Accepted: 28 August 2022

Published online: 24 September 2022

References

- Biel D, Brendel M, Rubinski A, Buerger K, Janowitz D, Dichgans M, et al. Tau-PET and in vivo Braak-staging as prognostic markers of future cognitive decline in cognitively normal to demented individuals. *Alzheimers Res Ther*. 2021;13(1):137.
- La Joie R, Visani AV, Baker SL, Brown JA, Bourakova V, Cha J, et al. Prospective longitudinal atrophy in Alzheimer's disease correlates with the intensity and topography of baseline tau-PET. *Sci Transl Med*. 2020;12(524):eaau5732.
- Ossenkoppele R, Smith R, Ohlsson T, Strandberg O, Mattsson N, Insel PS, et al. Associations between tau, A β , and cortical thickness with cognition in Alzheimer disease. *Neurology*. 2019;92(6):e601–12.
- Braak H, Braak E. Staging of Alzheimer's disease-related neurofibrillary changes. *Neurobiol Aging*. 1995;16(3):271–8 (discussion 8–84).
- Braak H, Braak E. Neuropathological staging of Alzheimer-related changes. *Acta Neuropathol*. 1991;82(4):239–59.
- Schöll M, Lockhart SN, Schonhaut DR, O'Neil JP, Janabi M, Ossenkoppele R, et al. PET imaging of tau deposition in the aging human brain. *Neuron*. 2016;89(5):971–82.
- Vogel JW, Iturria-Medina Y, Strandberg OT, Smith R, Levitis E, Evans AC, et al. Spread of pathological tau proteins through communicating neurons in human Alzheimer's disease. *Nat Commun*. 2020;11(1):2612.
- Pontecorvo MJ, Devous MD, Kennedy I, Navitsky M, Lu M, Galante N, et al. A multicentre longitudinal study of flortaucipir (18F) in normal ageing, mild cognitive impairment and Alzheimer's disease dementia. *Brain*. 2019;142(6):1723–35.
- Franzmeier N, Neitzel J, Rubinski A, Smith R, Strandberg O, Ossenkoppele R, et al. Functional brain architecture is associated with the rate of tau accumulation in Alzheimer's disease. *Nat Commun*. 2020;11(1):347.
- Jack CR Jr, Wiste HJ, Schwarz CG, Lowe VJ, Senjem ML, Vemuri P, et al. Longitudinal tau PET in ageing and Alzheimer's disease. *Brain*. 2018;141(5):1517–28.
- Ossenkoppele R, Iaccarino L, Schonhaut DR, Brown JA, La Joie R, O'Neil JP, et al. Tau covariance patterns in Alzheimer's disease patients match intrinsic connectivity networks in the healthy brain. *Neuroimage Clin*. 2019;23:101848.
- Franzmeier N, Dewenter A, Frontzkowski L, Dichgans M, Rubinski A, Neitzel J, et al. Patient-centered connectivity-based prediction of tau pathology spread in Alzheimer's disease. *Sci Adv*. 2020;6(48):eabd1327.
- van der Kant R, Goldstein LSB, Ossenkoppele R. Amyloid-beta-independent regulators of tau pathology in Alzheimer disease. *Nat Rev Neurosci*. 2020;21(1):21–35.
- Timmler S, Simons M. Grey matter myelination. *Glia*. 2019;67(11):2063–70.
- Grydeland H, Walhovd KB, Tamnes CK, Westlye LT, Fjell AM. Intracortical myelin links with performance variability across the human lifespan: results from T1- and T2-weighted MRI myelin mapping and diffusion tensor imaging. *J Neurosci*. 2013;33(47):18618–30.
- Yeatman JD, Wandell BA, Mezer AA. Lifespan maturation and degeneration of human brain white matter. *Nat Commun*. 2014;5:4932.
- Deoni SC, Dean DC 3rd, O'Muircheartaigh J, Dirks H, Jerskey BA. Investigating white matter development in infancy and early childhood using myelin water fraction and relaxation time mapping. *Neuroimage*. 2012;63(3):1038–53.
- Corrigan NM, Yarnykh VL, Hippe DS, Owen JP, Huber E, Zhao TC, et al. Myelin development in cerebral gray and white matter during adolescence and late childhood. *Neuroimage*. 2021;227:117678.
- Stricker NH, Schweinsburg BC, Delano-Wood L, Wierenga CE, Bangen KJ, Haaland KY, et al. Decreased white matter integrity in late-myelinating fiber pathways in Alzheimer's disease supports retrogenesis. *Neuroimage*. 2009;45(1):10–6.
- Bartzokis G. Age-related myelin breakdown: a developmental model of cognitive decline and Alzheimer's disease. *Neurobiol Aging*. 2004;25(1):5–18 (author reply 49–62).
- Bartzokis G, Lu PH, Mintz J. Human brain myelination and amyloid beta deposition in Alzheimer's disease. *Alzheimers Dement*. 2007;3(2):122–5.
- LoPresti P. Tau in Oligodendrocytes Takes Neurons in Sickness and in Health. *Int J Mol Sci*. 2018;19(8):2408.
- Cantuti-Castelvetri L, Fitzner D, Bosch-Queralt M, Weil MT, Su M, Sen P, et al. Defective cholesterol clearance limits remyelination in the aged central nervous system. *Science*. 2018;359(6376):684–8.
- Safaiyan S, Besson-Girard S, Kaya T, Cantuti-Castelvetri L, Liu L, Ji H, et al. White matter aging drives microglial diversity. *Neuron*. 2021;109(7):1100–17 e10.
- Depp C, Sun T, Sasmita AO, Spieth L, Berghoff SA, Steixner-Kumar AA, et al. Ageing-associated myelin dysfunction drives amyloid deposition in mouse models of Alzheimer's disease. *bioRxiv*. 2021:2021.07.31.454562.
- Braak H, Braak E. Development of Alzheimer-related neurofibrillary changes in the neocortex inversely recapitulates cortical myelogenesis. *Acta Neuropathol*. 1996;92(2):197–201.
- Liu H, Rubino C, Dvorak AV, Jarrett M, Ljungberg E, Vavasour IM, et al. Myelin Water Atlas: A Template for Myelin Distribution in the Brain. *J Neuroimaging*. 2019;29(6):699–706.
- Weiner MW, Veitch DP, Aisen PS, Beckett LA, Cairns NJ, Green RC, et al. The Alzheimer's Disease Neuroimaging Initiative 3: Continued innovation for clinical trial improvement. *Alzheimers Dement*. 2017;13(5):561–71.
- Franzmeier N, Rubinski A, Neitzel J, Kim Y, Damm A, Na DL, et al. Functional connectivity associated with tau levels in ageing, Alzheimer's, and small vessel disease. *Brain*. 2019;142(4):1093–107.

30. Landau SM, Mintun MA, Joshi AD, Koeppe RA, Petersen RC, Aisen PS, et al. Amyloid deposition, hypometabolism, and longitudinal cognitive decline. *Ann Neurol*. 2012;72(4):578–86.
31. Lowe VJ, Lundt ES, Albertson SM, Min H-K, Fang P, Przybelski SA, et al. Tau-positron emission tomography correlates with neuropathology findings. *Alzheimers Dement*. 2020;16(3):561–71.
32. Palmqvist S, Zetterberg H, Blennow K, Vestberg S, Andreasson U, Brooks DJ, et al. Accuracy of Brain Amyloid Detection in Clinical Practice Using Cerebrospinal Fluid β -Amyloid 42: A Cross-Validation Study Against Amyloid Positron Emission Tomography. *JAMA Neurol*. 2014;71(10):1282–9.
33. Mattsson N, Smith R, Strandberg O, Palmqvist S, Scholl M, Insel PS, et al. Comparing (18F)-AV-1451 with CSF t-tau and p-tau for diagnosis of Alzheimer disease. *Neurology*. 2018;90(5):e388–95.
34. Jagust WJ, Landau SM, Koeppe RA, Reiman EM, Chen K, Mathis CA, et al. The ADNI PET Core: 2015. *Alzheimer's Dementia*. 2015;11(7):757–71.
35. Avants BB, Tustison NJ, Song C, Cook PA, Klein A, Gee JC. A reproducible evaluation of ANTs similarity metric performance in brain image registration. *Neuroimage*. 2011;54(3):2033–44.
36. Schaefer A, Kong R, Gordon EM, Laumann TO, Zuo XN, Holmes AJ, et al. Local-Global Parcellation of the Human Cerebral Cortex from Intrinsic Functional Connectivity MRI. *Cereb Cortex*. 2018;28(9):3095–114.
37. Maass A, Landau S, Baker SL, Horng A, Lockhart SN, La Joie R, et al. Comparison of multiple tau-PET measures as biomarkers in aging and Alzheimer's disease. *Neuroimage*. 2017;157:448–63.
38. Baker SL, Maass A, Jagust WJ. Considerations and code for partial volume correcting [(18F)-AV-1451 tau PET data. *Data Brief*. 2017;15:648–57.
39. Smith R, Puschmann A, Scholl M, Ohlsson T, van Swieten J, Honer M, et al. 18F-AV-1451 tau PET imaging correlates strongly with tau neuropathology in MAPT mutation carriers. *Brain*. 2016;139(Pt 9):2372–9.
40. Glasser MF, Sotiropoulos SN, Wilson JA, Coalson TS, Fischl B, Andersson JL, et al. The minimal preprocessing pipelines for the Human Connectome Project. *Neuroimage*. 2013;80:105–24.
41. Braak H, Del Tredici K. Spreading of Tau Pathology in Sporadic Alzheimer's Disease Along Cortico-cortical Top-Down Connections. *Cereb Cortex*. 2018;28(9):3372–84.
42. Vogel JW, Young AL, Oxtoby NP, Smith R, Ossenkoppele R, Strandberg OT, et al. Four distinct trajectories of tau deposition identified in Alzheimer's disease. *Nat Med*. 2021;27(5):871–81.
43. Raj A, Kuceyeski A, Weiner M. A network diffusion model of disease progression in dementia. *Neuron*. 2012;73(6):1204–15.
44. Bartzokis G. Alzheimer's disease as homeostatic responses to age-related myelin breakdown. *Neurobiol Aging*. 2011;32(8):1341–71.
45. Chen JF, Liu K, Hu B, Li RR, Xin W, Chen H, et al. Enhancing myelin renewal reverses cognitive dysfunction in a murine model of Alzheimer's disease. *Neuron*. 2021;109(14):2292–307 e5.
46. Dean DC 3rd, Hurley SA, Kecskemeti SR, O'Grady JP, Canda C, Davenport-Sis NJ, et al. Association of Amyloid Pathology With Myelin Alteration in Preclinical Alzheimer Disease. *JAMA Neurol*. 2017;74(1):41–9.
47. Bulk M, Abdelmoula WM, Nabuurs RJA, van der Graaf LM, Mulders CWH, Mulder AA, et al. Postmortem MRI and histology demonstrate differential iron accumulation and cortical myelin organization in early- and late-onset Alzheimer's disease. *Neurobiol Aging*. 2018;62:231–42.
48. Mitew S, Kirkcaldie MT, Halliday GM, Shepherd CE, Vickers JC, Dickson TC. Focal demyelination in Alzheimer's disease and transgenic mouse models. *Acta Neuropathol*. 2010;119(5):567–77.
49. Nasrabady SE, Rizvi B, Goldman JE, Brickman AM. White matter changes in Alzheimer's disease: a focus on myelin and oligodendrocytes. *Acta Neuropathol Commun*. 2018;6(1):22.
50. Chen WT, Lu A, Craessaerts K, Pavie B, Sala Frigerio C, Corthout N, et al. Spatial Transcriptomics and In Situ Sequencing to Study Alzheimer's Disease. *Cell*. 2020;182(4):976–91 e19.
51. Brase L, You S-F, del Aguila J, Dai Y, Novotny BC, Soriano-Tarraga C, et al. A landscape of the genetic and cellular heterogeneity in Alzheimer disease. *medRxiv*. 2021:2021.11.30.21267072.
52. Schneider A, Araujo GW, Trajkovic K, Herrmann MM, Merkle D, Mandelkow EM, et al. Hyperphosphorylation and aggregation of tau in experimental autoimmune encephalomyelitis. *J Biol Chem*. 2004;279(53):55833–9.
53. Higuchi M, Zhang B, Forman MS, Yoshiyama Y, Trojanowski JQ, Lee VM. Axonal degeneration induced by targeted expression of mutant human tau in oligodendrocytes of transgenic mice that model glial tauopathies. *J Neurosci*. 2005;25(41):9434–43.
54. Couttas TA, Kain N, Suchowerska AK, Quek LE, Turner N, Fath T, et al. Loss of ceramide synthase 2 activity, necessary for myelin biosynthesis, precedes tau pathology in the cortical pathogenesis of Alzheimer's disease. *Neurobiol Aging*. 2016;43:89–100.
55. Klein C, Krämer E-M, Cardine A-M, Schraven B, Brandt R, Trotter J. Process Outgrowth of Oligodendrocytes Is Promoted by Interaction of Fyn Kinase with the Cytoskeletal Protein Tau. *J Neurosci*. 2002;22(3):698.
56. Seiwa C, Yamamoto M, Tanaka K, Fukutake M, Ueki T, Takeda S, et al. Restoration of FcRgamma/Fyn signaling repairs central nervous system demyelination. *J Neurosci Res*. 2007;85(5):954–66.
57. Briner A, Gotz J, Polanco JC. Fyn Kinase Controls Tau Aggregation In Vivo. *Cell Rep*. 2020;32(7):108045.
58. Safaiyan S, Kannaiyan N, Snaidero N, Brioschi S, Biber K, Yona S, et al. Age-related myelin degradation burdens the clearance function of microglia during aging. *Nat Neurosci*. 2016;19(8):995–8.
59. Ising C, Venegas C, Zhang S, Scheiblich H, Schmidt SV, Vieira-Saecker A, et al. NLRP3 inflammasome activation drives tau pathology. *Nature*. 2019;575(7784):669–73.
60. Nasrabady SE, Rizvi B, Goldman JE, Brickman AM. White matter changes in Alzheimer's disease: a focus on myelin and oligodendrocytes. *Acta Neuropathol Commun*. 2018;6(1):22.
61. Hansson O. Biomarkers for neurodegenerative diseases. *Nat Med*. 2021;27(6):954–63.
62. Fessel J. Reversing Alzheimer's disease dementia with clemastine, fingolimod, or rolipram, plus anti-amyloid therapy. *Alzheimers Dement (NY)*. 2022;8(1):e12242.
63. Najm FJ, Madhavan M, Zaremba A, Shick E, Karl RT, Factor DC, et al. Drug-based modulation of endogenous stem cells promotes functional remyelination in vivo. *Nature*. 2015;522(7555):216–20.
64. Cully M. Neurodegenerative diseases: Repurposing for remyelination. *Nat Rev Drug Discov*. 2015;14(6):383.
65. Mei F, Fancy SPJ, Shen YA, Niu J, Zhao C, Presley B, et al. Micropillar arrays as a high-throughput screening platform for therapeutics in multiple sclerosis. *Nat Med*. 2014;20(8):954–60.
66. Mei F, Lehmann-Horn K, Shen YA, Rankin KA, Stebbins KJ, Lorrain DS, et al. Accelerated remyelination during inflammatory demyelination prevents axonal loss and improves functional recovery. *Elife*. 2016;5:e18246.
67. Green AJ, Gelfand JM, Cree BA, Bevan C, Boscardin WJ, Mei F, et al. Clemastine fumarate as a remyelinating therapy for multiple sclerosis (ReBUILD): a randomised, controlled, double-blind, crossover trial. *Lancet*. 2017;390(10111):2481–9.
68. Xie YY, Pan TT, Xu DE, Huang X, Tang Y, Huang W, et al. Clemastine Ameliorates Myelin Deficits via Preventing Senescence of Oligodendrocytes Precursor Cells in Alzheimer's Disease Model Mouse. *Front Cell Dev Biol*. 2021;9:733945.
69. Moller HE, Bossoni L, Connor JR, Crichton RR, Does MD, Ward RJ, et al. Iron, Myelin, and the Brain: Neuroimaging Meets Neurobiology. *Trends Neurosci*. 2019;42(6):384–401.
70. Laule C, Kozlowski P, Leung E, Li DK, Mackay AL, Moore GR. Myelin water imaging of multiple sclerosis at 7 T: correlations with histopathology. *Neuroimage*. 2008;40(4):1575–80.
71. Laule C, Leung E, Li DK, Traboulsee AL, Paty DW, MacKay AL, et al. Myelin water imaging in multiple sclerosis: quantitative correlations with histopathology. *Mult Scler*. 2006;12(6):747–53.
72. Mancini M, Karakuzu A, Cohen-Adad J, Cercignani M, Nichols TE, Stikov N. An interactive meta-analysis of MRI biomarkers of myelin. *Elife*. 2020;9:e61523.
73. Papadaki E, Kavroulakis E, Kalaitzakis G, Karageorgou D, Makrakis D, Maris TG, et al. Age-related deep white matter changes in myelin and water content: A T(2) relaxometry study. *J Magn Reson Imaging*. 2019;50(5):1393–404.
74. Dao E, Tam R, Hsiung GR, Ten Brinke L, Crockett R, Barha CK, et al. Exploring the Contribution of Myelin Content in Normal Appearing White Matter to Cognitive Outcomes in Cerebral Small Vessel Disease. *J Alzheimers Dis*. 2021;80(1):91–101.
75. Kavroulakis E, Simos PG, Kalaitzakis G, Maris TG, Karageorgou D, Zaganas I, et al. Myelin content changes in probable Alzheimer's disease and mild cognitive impairment: Associations with age and severity of neuropsychiatric impairment. *J Magn Reson Imaging*. 2018;47(5):1359–72.

Publisher's Note

Springer Nature remains neutral with regard to jurisdictional claims in published maps and institutional affiliations.